Statics and dynamics of polymeric droplets on chemically homogeneous and heterogeneous substrates

Ö. Öztürk* and J. Servantie†

Department of Physics, Istanbul Technical University, Maslak 34469, Istanbul, Turkey

(Received 8 May 2019; revised manuscript received 24 July 2019; published 22 August 2019)

We present a molecular dynamics study of the motion of cylindrical polymer droplets on striped surfaces. We first consider the equilibrium properties of droplets on different surfaces, we show that for small stripes the Cassie-Baxter equation gives a good approximation of the equilibrium contact angle. As the stripe width becomes nonnegligible compared to the dimension of the droplet, it has to deform significantly to minimize its free energy; this results in a smaller value of the contact angle than the continuum model predicts. We then evaluate the slip length and thus the damping coefficient as a function of the stripe width. For very small stripes, the heterogeneous surface behaves as an effective surface, with the same damping as a homogeneous surface with the same contact angle. However, as the stripe width increases, damping at the surface increases until reaching a plateau. Afterwards, we study the dynamics of droplets under a bulk force. We show that if the stripes are large enough the droplets are pinned until a critical force. The critical force increases linearly with stripe width. For large enough forces, the average velocity increases linearly with the force, we show that it can then be predicted by a model depending only on droplet size, contact angle, viscosity, and slip length. We show that the velocity of the droplet varies sinusoidally as a function of its position on the substrate. However, for bulk forces just above the depinning force we observe a characteristic stick-slip motion, with successive pinnings and depinnings.

DOI: 10.1103/PhysRevE.100.023113

I. INTRODUCTION

The wetting behaviors of liquid volumes ranging from microliters to picoliters in microchannels are of great importance for designing droplet-based microfluidic devices [1–3], such as DNA-chips [4], Lab On A CD [5], inkjet printing technology [6], or *in situ* investigation of fibrin networks [7]. Accordingly, equilibrium and dynamic wetting behaviors of liquid drops on smooth (ideal, homogeneous, flat), chemically rough/structured, and topologically patterned substrates has been studied for decades [8–17].

Furmidge [8] showed that the movement of spray liquids on different substrates depends on the droplet's size, inclination of the substrate, the surface tension of the drop, and the advancing and receding contact angles. Gau *et al.* [10] showed that a shape instability (a bulge state), unlike a Rayleigh Plateau instability, can be employed for all liquids on all striped substrates if the hydrophilic stripes' contact angles are small enough and if these stripes are long enough. They mentioned that these bulge states could be used to build two-dimensional microchannel networks and hence to construct microbridges, microchips, and microreactors.

To date many experimental [18–24], computational, and theoretical [25–38] studies on the dynamic wetting behavior of droplets on textured surfaces have shown that a stick-slip type of motion is a common behavior.

Schäffer and Wong [18] showed that surface roughness is a key factor in pinning of water in glass capillaries. Léopoldès and Bucknall [19] studied the spreading of droplets on chemically heterogeneous striped substrates. In an intermediate regime, they observed a stick-slip behavior, in other words, a sudden hopping while crossing the boundary of two adjacent stripes with different wettability. Tavana *et al.* [20] investigated different organic (*n*-alkanes) drops on two distinct polymeric films. They observed that on homogeneous surfaces, all the liquids moved smoothly, whereas on heterogeneous polymeric films, liquids which have compounds with short-chains present stick-slip. They suggested that the cause of this stick-slip pattern is the varying adsorption of vapor molecules on these polymer films. Maheshwari *et al.* [21] observed a pinning-depinning cyclic behavior of DNA solutions at high and intermediate DNA concentrations. Similarly, Orejon *et al.* [22] observed that the magnitude of the stick-slip motion depends on the concentration of titanium dioxide nanoparticles inside water drops on different hydrophobic substrates. Yeong *et al.* [24] investigated the three-phase contact line dynamics of water droplets on superhydrophobic substrates with regular textured pillars. They proposed that the receding contact line undergoes a "slide-snap behavior." Here, the receding contact line keeps moving on a pillar until snapping to the adjacent pillar, in contrast to a stick-slip motion in which the contact line stays pinned before jumping into the consecutive locations.

Computational and theoretical investigations can also be summarized as follows. Shanahan [25] calculated the excess free energy of an evaporating drop. The model suggests the radius of the drop decreases smoothly on a homogeneous surface while stick-slip can occur on surfaces with heterogeneities. Thiele and Knobloch [26,27] studied the dynamics

*ozlemozturk@itu.edu.tr
†cservantie@itu.edu.tr

of two-dimensional droplets on heterogeneous surfaces by solving the Navier-Stokes equation within the long-wave approximation. They observed two kinds of pinnings can occur. A hydrophilic defect at the back of the drop or a hydrophobic at the front, leading to two different bifurcations. Beltrame *et al.* [32] obtained similar results for three-dimensional droplets. Kusumaatmaja *et al.* [28,29] studied the dynamics of two and three dimensional droplets thanks to lattice Boltzmann simulations (LB) [39], they observed slip, stick, and jumps of the contact line and important periodic variation in the shape of the droplet. Wang *et al.* [30] carried on continuum simulations of contact line dynamics of two immiscible fluids between two chemically patterned substrates using a diffuse-interface model with the generalized Navier boundary condition. Their results suggest a oscillations in the velocity of the contact line, with stick-slip behavior depending on the wettability contrast. Furthermore, they observed an increase in dissipation as the wettability contrast increases. Similar results were reported by Qian *et al.* [31] with MD simulations. Herde *et al.* [33] studied the depinning/pinning dynamics of two-dimensional drops driven on surfaces with sinusoidal wetting patterns. They solved the Navier Stokes equation using the boundary element method with slip boundary condition. Their results suggest an increase in the minimum force to depin the droplet with the wettability contrast. Furthermore, after the depinning slippage at the boundary can reduce the dissipation significantly. Sbragaglia and coworkers [34,35] observed a stick-slip periodic behavior for liquid drops sliding over substrates patterned with parallel stripes of varying wettability degrees both experimentally and numerically in two dimensions. They solved the diffuse-interface Navier-Stokes equations of motion for a binary mixture thanks to LB simulations. Their results suggest periodic increases in the fluctuations at the contact lines leading to dissipation of energy localized in time. Recent MD simulations on the evaporation of droplets on patterned surfaces also suggest a stick-slip dynamics of the contact line [36]. Though, according to Zhang *et al.* [37] one should look to the sticking as an extreme slow down instead of a pinning. While most studies observe some kind of stick-slip motion, it is unclear if the droplet remains pinned or slow downs, or what is the contribution to the dissipation of the oscillatory motion. The aim of this work is to study these problems thanks to a coarse-grained MD simulations and an analytical model we developed previously for droplets on homogeneous surfaces [12].

This paper is organized as follows: In Sec. II, we describe the details of the coarse grained model and the MD simulation we use. Then, in Sec. III we study the equilibrium and dynamic properties of polymeric droplets on homogeneous and heterogeneous surfaces. The conclusions are finally drawn in Sec. IV.

II. THE COARSE-GRAINED MD MODEL

In this paper, we use a generic particle-based molecular dynamics (MD) simulation technique to study the static and dynamic wetting behaviors of polymer droplets on different substrates [40–42]. Thanks to this coarse-grained model one can investigate the universal wetting properties of polymeric droplets on corrugated or smooth substrates. In this model, a bead of a linear homopolymer chain corresponds to a group of united molecules or atoms. The main advantage of using polymer melts in MD simulations is due to the fact that their vapor pressure is very low [12,43]. Hence, the number of atoms in the vapor phase remains small permitting the study of larger systems.

The polymer melt is modeled with bonded (intramolecular) and nonbonded (intermolecular) interactions. The bonded interactions are between neighboring beads of a polymer, it is modeled by the finitely extensible nonlinear elastic (FENE) potential [40,41],

$$U_{\mathrm{FENE}} = \begin{cases} -\frac{1}{2}kR_0^2 \ln\left[1-\left(\frac{r}{R_0}\right)^2\right] & \text{for } r < R_0, \\ \infty & \text{for } r \geqslant R_0, \end{cases} \tag{1}$$

where the spring constant is $k = 30\epsilon/\sigma^2$ and the maximum covalent bond length $R_0 = 1.5\sigma$. Thanks to the FENE potential, the connectivity of the beads along the backbone chain is obtained. In addition to the bonded potential, there is a 12-6 Lennard-Jones (LJ) potential between each pair of beads in the system,

$$U_{\mathrm{LJ}} = \begin{cases} 4\epsilon\left[\left(\frac{\sigma}{r}\right)^{12} - \left(\frac{\sigma}{r}\right)^{6}\right] & \text{for } r < r_c, \\ 0 & \text{for } r \geqslant r_c, \end{cases} \tag{2}$$

where the cut-off distance is $r_c = 2 \times 2^{1/6}\sigma$. The repulsive part of the Lennard-Jones interaction permits to enforce the excluded volume effect while the attractive part permits to have a liquid state. The system is prepared so that each polymer contains $N_p = 10$ identical atoms of mass m.

The surface is modelled by two rigid layers of face-centered-cubic lattice. The number density of the substrate is chosen as $\rho_s = 2.0\sigma^{-3}$ [12]. Large enough so that no polymer atoms go through the surface. The atoms of the substrate interact with the polymeric fluid with a modified Lennard-Jones potential [44],

$$U_s = \begin{cases} 4\epsilon_s\left[\left(\frac{\sigma_s}{r}\right)^{12} - C_s\left(\frac{\sigma_s}{r}\right)^{6}\right] & \text{for } r < r_c, \\ 0 & \text{for } r \geqslant r_c, \end{cases} \tag{3}$$

where the cut-off distance is the same as in Eq. (2). The length and energy scales of the potential energy are fixed to $\sigma_s = \sigma$ and $\epsilon_s = \epsilon$, respectively. Finally, the empirical parameter C_s quantifies the hydrophobicity of the surface. The larger C_s is, the more attractive and consequently, hydrophilic the substrate is. Thus, one can easily tune the wetting properties of the surface. Furthermore, one can construct a simple heterogeneous surface by alternating the type of atom by using different hydrophobicity parameter C_s. We prepare surfaces with increasing stripe width. The hydrophobicity parameters are fixed to $C_s = 0.4$ (hydrophobic surface) and $C_s = 0.6$ (hydrophilic surface). All the surfaces have a total of 11520 atoms and the dimensions $L_x = 241.90489$ (longitudinal to the flow), $L_y = 18.9\sigma$ (transverse to the flow). Periodic boundaries are enforced in the x and y directions, while reflective periodic boundaries are in effect on the top of the simulation box in the z direction. The height of the simulation box along the z axis is taken large enough for the droplet's upper part not to touch the box, therefore one can obtain a free liquid surface, namely, $L_z = 150.0\sigma$. The equations of motion are integrated with the velocity Verlet algorithm [45] with a time step of $\Delta t = 0.005\tau$. We fix the temperature of the system to

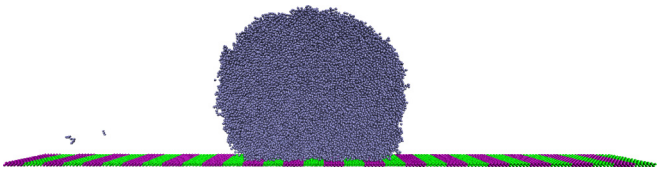

FIG. 1. MD simulation snapshot of a droplet at equilibrium. The droplet of $N = 50\,000$ atoms is on a striped surface having two types of atoms with $C_s = 0.4$ (green) and $C_s = 0.6$ (purple). The stripes have and equal widths of $w = 7.56\sigma$. The atoms on the left-hand side of the figure are in the extremely low vapor phase of the polymeric fluid.

$k_BT = 1.2\epsilon$ for all the MD simulations, at this temperature the density of the polymer melt is $\rho_p = 0.788\sigma^{-3}$ and the vapor density is negligible [46,47]. We prepare the polymer droplet by first constructing a cubical lattice of polymers, once the cube is equilibrated we place it on the substrate and equilibrate again. We depict in Fig. 1 an equilibrated droplet of $N = 50\,000$ monomers on a heterogeneous surface with stripe width $w = 7.56\sigma$. The equilibrium contact angle of the droplet is $\theta_E = 133^\circ$. Finally, a dissipative particle dynamics (DPD) [12,48,49] thermostat is used to keep the temperature of the system constant. The DPD thermostat has the advantage of conserving the momentum locally instead of globally as for the Nosé-Hoover thermostat [48–50]. The damping coefficient of the thermostat is set to $0.5\tau^{-1}$ in all our simulations.

III. RESULTS

A. Equilibrium wetting properties

We calculate the equilibrium contact angles, θ_E, of droplets for various strengths of the hydrophobicity parameter, C_s, and droplet sizes, N. We focus on cylindrical droplets to study larger liquid systems and have better statistics. We use droplet sizes from $N = 10\,000$ to $N = 50\,000$ monomers and hydrophobicity parameters in the range $C_s = 0.3$–0.8 to study the equilibrium density profiles. The density profiles are obtained by counting the number of monomers in two-dimensional boxes of size 0.1σ in the x and z directions. We choose the contour line as the arithmetic mean of the densities of the polymer melt and its vapor, since the density of the vapor is negligible, the contour line corresponds to a density of $\rho_p/2 = 0.394\sigma^{-3}$. We depict in Fig. 2 the density profiles for increasing number of monomers with the hydrophilic parameter set to $C_s = 0.5$. Becker *et al.* showed that the contact angle is independent of the size of the droplet for large enough systems, namely, $N = 10\,000$ [51]. We can thus evaluate the angle precisely by using drops of different sizes and evaluate their average [12]. The geometry of cylindrical droplets at equilibrium satisfy the following relationships,

$$V = \frac{R^2}{2}(2\theta_E - \sin 2\theta_E)L_y, \tag{4}$$

$$A = 2R\sin\theta_E Ly, \tag{5}$$

$$H = R(1 - \cos\theta_E), \tag{6}$$

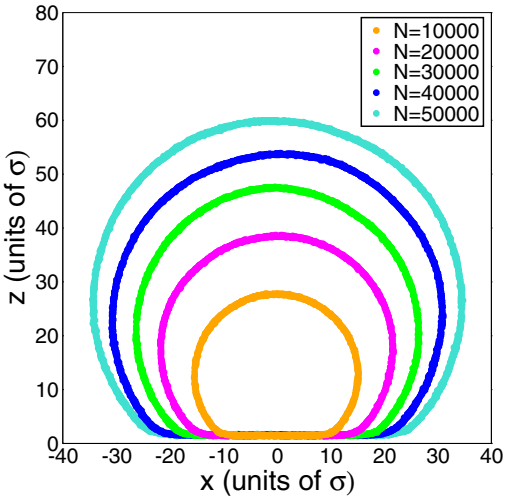

FIG. 2. Density profiles for increasing number of monomers. The surface is homogeneous with hydrophobic parameter $C_s = 0.5$. The average equilibrium contact angle of these droplets is $\theta_E = 137^\circ \pm 1^\circ$.

$$r_z = R\left(\frac{4}{3}\frac{\sin^3\theta_E}{2\theta_E - \sin 2\theta_E} - \cos\theta_E\right), \tag{7}$$

where V, H, A, and r_z are, respectively, the volume, the height, the area of contact with the substrate, and height of the center of mass. The height of the center of mass is readily available in MD simulations. Then, using the contour plots in Fig. 2 we fit circles to the droplets to find the radius of the droplet R. One can then solve Eq. (7) numerically to find θ_E. The same procedure is applied for varying hydrophobicity parameters C_s. We depict in Fig. 3 the density profiles of a droplet of $N = 30\,000$ monomers for increasing values of C_s. As expected, increasing the strength of the attractive part of the interaction potential results in a more hydrophilic surface, and thus a lower contact angle. The inset of Fig. 3 depicts the equilibrium contact angle as a function of C_s. We remark

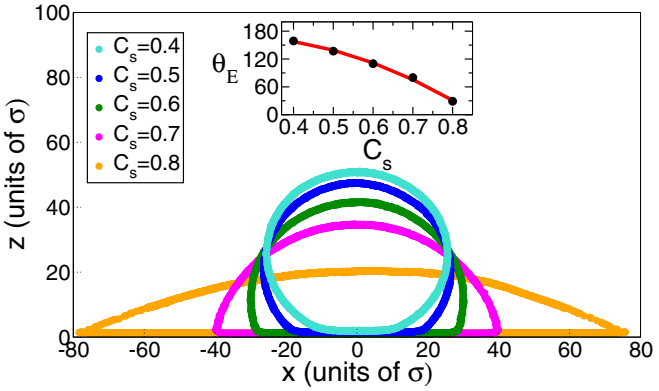

FIG. 3. Density profiles of droplets with $N = 30\,000$ atoms for increasing values of the hydrophobicity parameter C_s. The surfaces are chemically homogeneous substrates. The inset represents the equilibrium contact angle as a function of C_s. The contact angle is given in degrees.

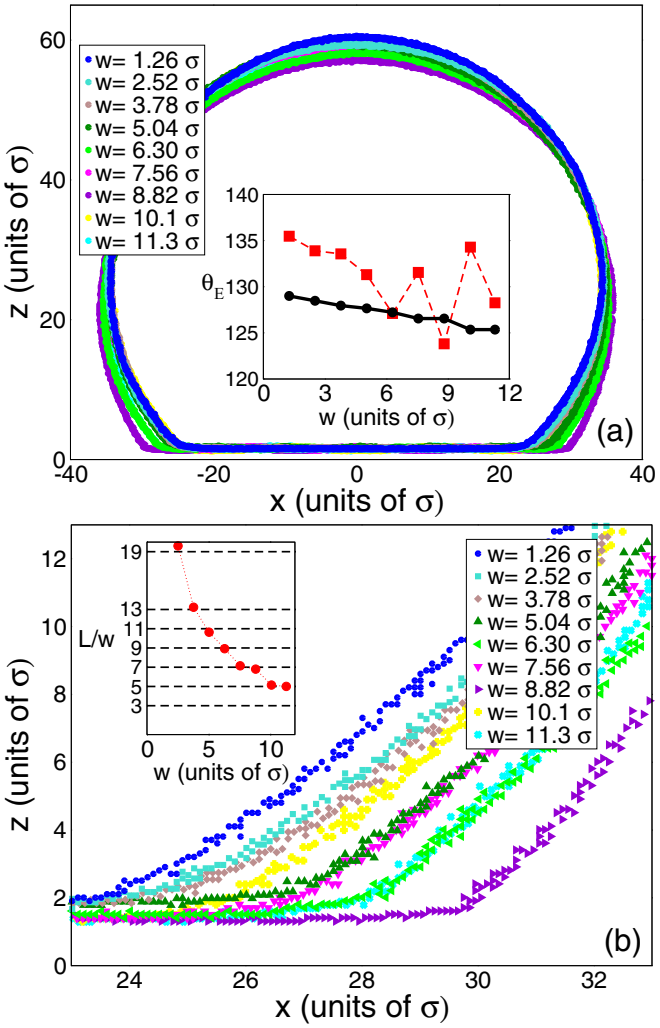

FIG. 4. (a) Density profiles of a droplet of $N = 50\,000$ atoms on different striped substrates. The circles in the inset represent the Cassie-Baxter angle, and the squares the actual equilibrium contact angle as a function of the stripe width w. (b) Close up view of the contact line for the different droplets, the inset depicts the length of the droplet divided by the stripe width w as a function of w.

that the super-hydrophobic surfaces we observe for $C_s < 0.6$ cannot be achieved experimentally without surface roughness, indeed it is well known that the maximum contact angle of water on a smooth surface is approximately of 120° [52]. As such these results are purely numerical and cannot be compared to experimental results directly.

We now focus on the striped surfaces. We choose the value $C_s = 0.4$ ($\theta_E = 159°$) for the hydrophobic stripe and $C_s = 0.6$ ($\theta_E = 110°$) for the hydrophilic one. This corresponds to a wettability contrast of 49°, comparable to the one used by Zhang *et al.* [37] (48°) albeit with a larger contact angle in our case. We compute the equilibrium density profile of a droplet of $N = 50\,000$ atoms on surfaces of varying stripe widths $w = 1.26,\ 2.52,\ 3.78,\ 5.04,\ 6.30,\ 7.56,\ 8.82,\ 10.08,\ 11.34\sigma$. These values correspond to the stripe width to droplet length ratios of $w_p = 3,\ 5,\ 8,\ 10,\ 13,\ 15,\ 18,\ 20,\ 23\%$. We depict in Fig. 4 the density profiles. The inset of Fig. 4(a) represents the equilibrium contact angles, and the contact angle corresponding to the Cassie-Baxter equation as a function of stripe width. The Cassie-Baxter equation [53], is a continuum result, it predicts the equilibrium contact angle of a droplet on a mixed surface as,

$$\cos\theta_{\rm CB} = f_1 \cos\theta_1 + f_2 \cos\theta_2, \tag{8}$$

where f_1 and f_2 are, respectively, the contact area fractions of the surface of type 1 and 2, and θ_1 and θ_2 their respective equilibrium contact angles. We notice that, the calculated value θ_E is close to the continuum prediction $\theta_{\rm CB}$. Indeed, on average we obtain $\theta_E = 131° \pm 4°$ for the equilibrium contact angle, while the data for the homogeneous surfaces and $f_1 = f_2 = 0.5$ yields $\theta_{\rm CB} = 127 \pm 1°$. However, we notice that the contact angle decreases with the stripe width and varies wildly at large values of w. This is due to the fact that at equilibrium the droplet maximizes its contact area with the hydrophilic stripes to minimize the free energy. To achieve this the droplets slightly deforms to be in contact with one more hydrophilic stripe than hydrophobic stripes. In that case, the droplet has to be in contact with an odd number of stripes. As the stripe width increases, to accommodate an odd number of stripes, the droplet has to deform significantly, resulting in the important variation of the contact angle. We have depicted in Fig. 4(b) a close up on the contact line for all the different striped surfaces. In the inset we give the contact length to stripe width ratio. As we see, the length of the droplet varies as an odd number times the stripe width. In general, the fact that there is an extra hydrophilic stripe with respect to the hydrophobic one will make the surface effectively more hydrophilic, and hence with a lower contact angle. As the stripe width increases, the effect becomes more important, thus the contact angle will decrease with w. We remark that we have taken this effect into account while evaluating the Cassie-Baxter contact angle in Fig. 4(a).

B. Boundary condition

Before considering the dynamics of droplets on the different surfaces one has to evaluate the boundary condition. Indeed, we showed previously that for microscopic droplets the presence of slip at the surface can significantly affect the dynamics of the droplets. Specifically, for small droplets and large contact angles the slipping on the surface becomes the dominating dissipation mechanism leading to an increased velocity [12]. In the presence of slippage at the boundary one can use the Navier slip boundary condition [54],

$$\eta \frac{\partial v_x}{\partial z}\bigg|_{z_b} = \lambda v_b, \tag{9}$$

where η is the shear viscosity, z_b is the position of the boundary, λ a damping coefficient quantifying the friction at the surface, and v_b the velocity of the fluid on the surface. We previously evaluated the shear viscosity thanks to the Green-Kubo relationship to be $\eta = 5.3 \pm 0.1\ \sigma^2/\sqrt{m\epsilon}$ [12]. The damping coefficient can also be evaluated thanks to a Green-Kubo relationship, namely [55,56],

$$\lambda = \frac{1}{k_B T A} \int_0^\infty dt\ \langle F_s(t) F_s(0) \rangle, \tag{10}$$

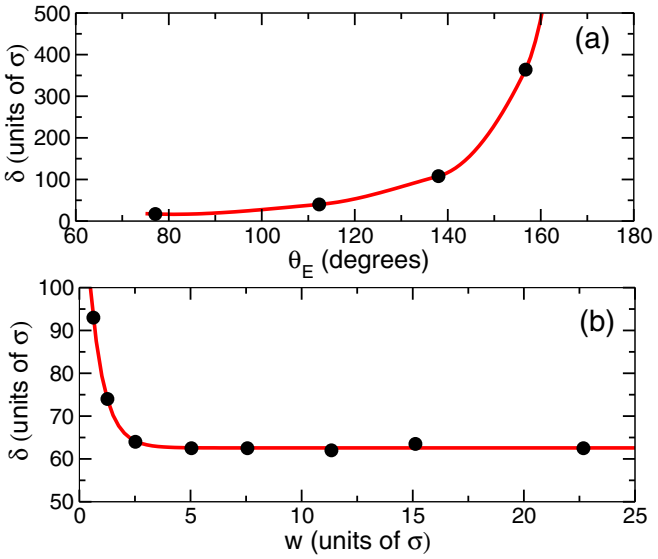

FIG. 5. (a) Slip length as a function of the equilibrium contact angle for homogeneous surfaces. (b) Slip length as a function of the stripe width. The solid lines are guides for the eyes.

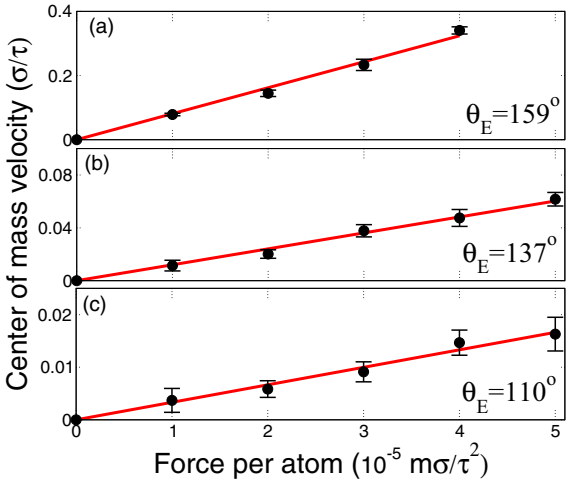

FIG. 6. Time-averaged velocity of the center of mass in the longitudinal direction for droplets of $N = 50\,000$ monomers as a function of the force per atom for homogeneous surfaces. The circles are the results of the MD simulations and the plain lines are linear fits.

where F_s is the tangential force exerted by the substrate on the fluid, and A is the area of contact. The slip length is then given as

$$\delta = \frac{\eta}{\lambda}. \tag{11}$$

To evaluate δ we confine a fluid with $N = 50\,000$ monomers between two surfaces with $L_x = 90.7\sigma$ and $L_y = 18.9\sigma$. The distance between the surfaces is tuned to recover the bulk liquid density far from the walls. After equilibration, we compute the total transverse force for 4×10^6 time steps and evaluate its time autocorrelation. Finally, the slip length is obtained thanks to Eqs. (10) and (11). We depict the results in Fig. 5. For homogeneous surfaces we notice a sharp increase of δ as a function of the equilibrium contact angle θ_E. This result is consistent with the constant relative atom size we consider in this study ($\sigma_r = \sigma_s/\sigma$) [57,58]. For all the contact angles considered we notice that the slip length is important compared to the dimensions of the droplet. Consequently, we expect slippage to be the dominating mechanism of dissipation on the homogeneous surfaces. However, for the heterogeneous surfaces for very small stripe widths we recover the value of δ corresponding to the homogeneous case, i.e., for a contact angle of $\theta \approx 130^\circ$ about $\delta \approx 90\ \sigma$. As the stripe width increases the slip length decreases and rapidly reaches a plateau at $\delta \approx 60\ \sigma$. The plateau is reached at approximately $3.5\ \sigma$, close to the effective size of the polymers. Indeed, the end-to-end distance of the polymers is found to be $R_{ee} = 3.447\ \sigma$. For very small stripe widths the stripes merge to an effective surface with an equilibrium contact angle corresponding to the Cassie-Baxter relation, as the stripe width increase the polymers interacts with the two distinct surfaces, leading to increased fluctuations at their boundaries, and consequently increased damping λ, therefore decreased slip length δ. Once the stripes become larger than the polymers, the increased damping remains confined to the boundary between stripes, and thus a plateau is reached. A similar decrease was predicted by Priezjev *et al.* by solving the Navier-Stokes equation for a fluid confined between a homogeneous wall and a striped wall [59]. We note that the slip length is important for both the homogeneous and heterogeneous surfaces, this is due to the fact that even though the striped surfaces are chemically heterogeneous they are still smooth.

C. Dynamic wetting properties

In this section we focus on the dynamics of the cylindrical polymer droplets on the homogeneous and heterogeneous substrates. We first study the homogeneous surfaces. We consider three different hydrophobicity parameter $C_s = 0.4,\ 0.5,\ 0.6$ which corresponds to the equilibrium contact angles $\theta_E = 159^\circ,\ 137^\circ,\ 110^\circ$. To have a sustained motion we apply a bulk force F in the longitudinal direction x to all the fluid atoms. The calculations are carried out for an equilibrated droplet of $N = 50\,000$ monomers. We use five different values of the bulk force per atom, namely, $F = 0.00001,\ 0.00002,\ 0.00003,\ 0.00004,\ 0.00005$. After 2×10^6 time steps of equilibration, a nonequilibrium steady state is reached. We then compute the time average of the velocity of the center mass in the longitudinal direction, $\langle v_{CM} \rangle$ for a further 2×10^6 time steps. We depict the results in Fig. 6. We showed previously [12] that the velocity profile in cylindrical droplets can be estimated by

$$v_x(z) = \frac{\rho_p}{\eta}\left[\left(H - \frac{z}{2}\right)z + \delta H\right]\frac{F}{m}, \tag{12}$$

where H is the height of the droplet and δ the slip length. Thus, the velocity of the center of mass can then be written as

$$v_{CM} = \frac{\rho_p}{\eta}\left[\left(H - \frac{r_z}{2}\right)r_z + \delta H\right]\frac{F}{m}. \tag{13}$$

This relationship was derived thanks to the lubrication approximation. It is valid as long as there is slippage and the

TABLE I. Molecular dynamics simulation results for polymer droplets of $N = 50\,000$ atoms on chemically homogeneous surfaces for the three hydrophobicity parameter C_s. γ corresponds to the effective damping coefficient evaluated thanks to Eq. (13) and γ_{MD} the one obtained from the linear fits in Fig. 6.

C_s	θ_E	$r_z\,(\sigma)$	$H\,(\sigma)$	$\delta(\sigma)$	$\gamma\,(m/\tau)$	$\gamma_{\mathrm{MD}}\,(m/\tau)$
0.4	159°	31	63	364	14	6
0.5	137°	27	58	108	45	41
0.6	110°	23	52	40	112	150

droplet is not deformed significantly, i.e., for small contact angle hysteresis. Indeed, it is well known that drops have first to overcome the capillary force to start sliding [8,60,61]. Since the velocity of the center of mass scales linearly with the bulk force, to validate Eq. (13) with the MD simulations, one can simply assume the velocity of the center of mass satisfies the following equation of motion,

$$m_{\mathrm{CM}}\frac{dv_{\mathrm{CM}}}{dt} = -\gamma_{\mathrm{MD}}\,v_{\mathrm{CM}} + m_{\mathrm{CM}}\frac{F}{m}, \tag{14}$$

where the effective damping coefficient γ_{MD} comprises all the different types of dissipation present in the droplet, namely, viscous dissipation in the volume, frictional dissipation at the surface, and dissipation at the contact line. At the steady state the expectation value of the center of mass velocity can then be written as

$$v_{\mathrm{CM}} = \frac{\rho_p V}{\gamma_{\mathrm{MD}}}\frac{F}{m}. \tag{15}$$

Performing linear fits on the data in Fig. 6 permits to evaluate the effective dissipation coefficient γ_{MD}. One can then compare it to the prediction from Eq. (13), γ. We present the results of the fits, and the prediction of the damping coefficient according to Eq. (13) in Table I.

We notice that apart for $C_s = 0.4$ Eq. (13) gives a relatively good approximation of the damping coefficient. Errors come from two different approximation; first, Eq. (13) is valid only when the contact angle is not too large, second, to evaluate the slip length with Eq. (11) one needs the local viscosity, i.e., the viscosity at the surface. It is known that the mobility of the fluid in the vicinity of the substrate is affected by the substrate and consequently its viscosity [43].

We previously looked to the size dependence of the steady-state velocity [12]. For small droplets the dominating dissipation mechanism is the friction at the surface, in that case $v_{\mathrm{CM}} \sim R$. However, for large droplets the dominating dissipation mechanism is viscous dissipation in the volume, then $v_{\mathrm{CM}} \sim R^2$. In general, the velocity increases with size. Unfortunately, one can not write a simple scaling law for the dependence on contact angle from Eq. (13). Instead, one can look to the velocity at the top of the droplet $z = H$,

$$v_{\mathrm{top}} = \frac{\rho_p F}{m\eta}\left(\frac{H}{2} + \delta\right)H. \tag{16}$$

For droplets of fixed volume one can then get two limiting cases. For small droplets or a large slip length compared to its height the velocity at the top scales as $v_{\mathrm{top}} \sim \delta H$. While for large droplets or a small slip length compared its size one has

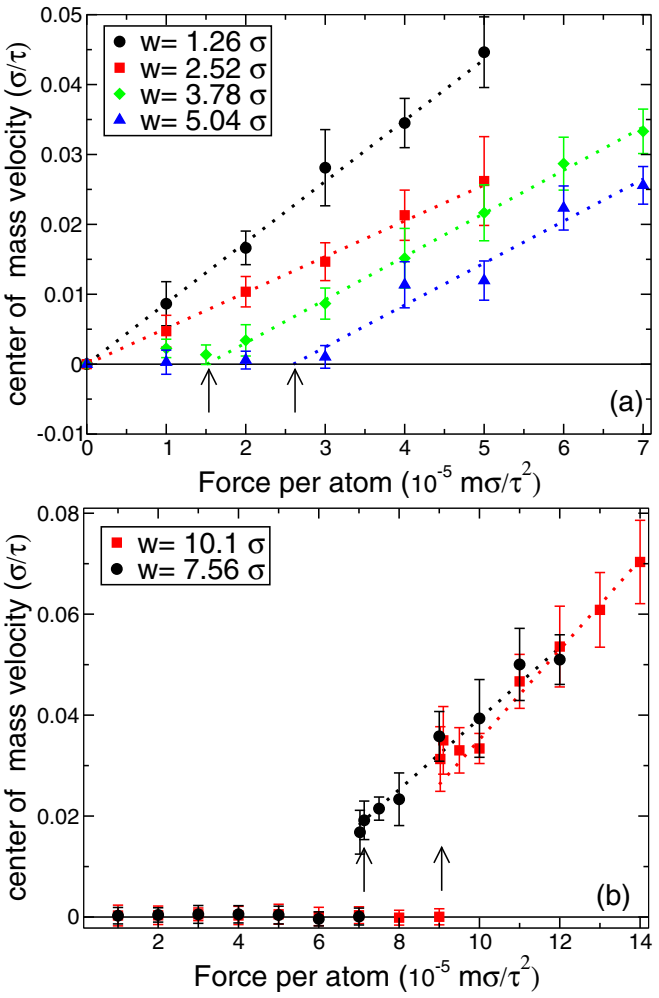

FIG. 7. Time average of the velocity of the center of mass of droplets with $N = 50\,000$ monomers as a function of the force per atom for the chemically heterogeneous surfaces. (a) $w = 1.26$–$5.04\ \sigma$ and (b) $w = 7.56\sigma$ and $w = 10.1\ \sigma$. The symbols correspond to the results of the MD simulations and the dotted lines to linear fits. The arrows point to the depinning force.

$v_{\mathrm{top}} \sim H^2$. Notice that the height of a cylindrical droplet can be expressed as

$$H = \sqrt{\frac{2V}{L_y}}\frac{1-\cos\theta_E}{\sqrt{2\theta_E - \sin 2\theta_E}}, \tag{17}$$

which is a monotonically increasing function of the contact angle. Thus, the steady-state velocity of the droplet increases with its contact angle. As the surface becomes more hydrophobic, the shape of droplet becomes more like a sphere, which reduces the viscous damping during the rolling motion.

We now focus on the chemically heterogeneous substrates. We consider the droplets in Fig. 4 and drive them with varying bulk forces F. We depict the time averaged velocity of the center mass as a function of the force per atom for the different values of w in Fig. 7.

For the two smallest stripe widths, namely, $w = 1.26\ \sigma$ and $w = 2.52\ \sigma$ the velocity of the center of mass is still a linear function of the bulk force. However, as the stripe width

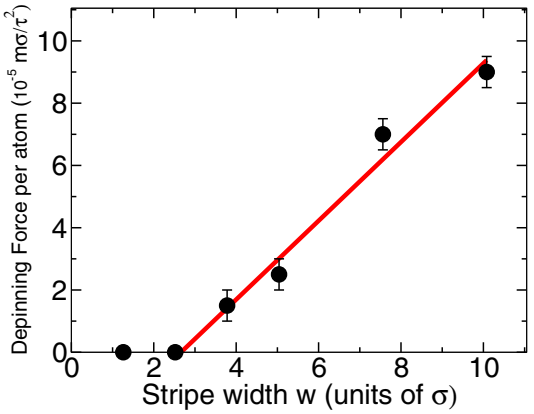

FIG. 8. The depinning force per atom as a function of the stripe width w. The circles are the results from the MD simulations and the solid line a linear fit on the nonzero values of the depinning force per atom.

increases we notice that a minimum force is required for a sustained motion, in other words the droplet remains pinned. Lets first focus on the pinned state. We notice that as the stripe width increases the minimum force increases. Herde *et al.* [33] observed the same behavior albeit for increasing wettability contrasts instead of stripe width. Increasing stripe width or the wettability contrast both result in increasing the heterogeneity of the surface, and hence the energy barrier the droplet must cross. Furthermore, experimental results by Mirsaidov *et al.* [23] showed that small droplets would remain pinned while large droplets could slide, as the droplet size decreases, surface heterogeneities become large with respect to the droplet size.

Using the results in Fig. 7, we depict the critical force per atom in Fig. 8. We notice that except for very small stripe widths, the depinning force increases linearly with stripe width. For small widths the energy barrier the droplet must cross is relatively small, consequently, thermal fluctuations are enough to overcome it. Remark that for stripe widths $w \geqslant 11.34\ \sigma$ the droplet can not depin without significant contact angle hysteresis. It corresponds to stripe width to droplet length ratios larger than 23%. However, the linear increase of the depinning force can be explained easily by a qualitative argument. Indeed, when the droplet is pinned it maximizes its contact area with the hydrophilic stripes to minimize its free energy. One can see this effect clearly from the density fluctuations in pinned droplets in Fig. 9. To maximize its contact with the hydrophilic stripes, each extremity of the droplet has to be on a hydrophilic stripe. In that case, if the droplet is in contact with n hydrophobic stripes, then it will be in contact with $n+1$ hydrophilic ones. Since there is slippage at the surface the whole contact area of the droplet moves instead of only the contact line. Assuming that $+W_s$ is the work required to move the fluid from a hydrophilic stripe to a hydrophobic one, then $-W_s$ is the work for the fluid moving from a hydrophobic stripe to a hydrophilic. Since there is an extra hydrophilic stripe there will remain a net work $+W_s$ to depin the droplet as schematized in Fig. 10. The depinning work W_s depends on the difference of surface energies Δe per unit area and on

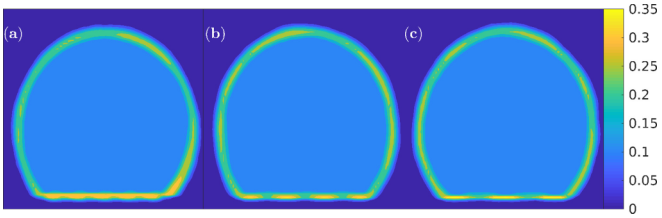

FIG. 9. Density fluctuations of a pinned droplet with a bulk force per atom $F = 0.00001\ (m\sigma/\tau^2)$. (a) $w = 5.04\ \sigma$, (b) $w = 7.56\ \sigma$ and (c) $w = 10.1\ \sigma$. The contour maps correspond to the standard deviation of the number density averaged over 2×10^6 simulation time steps.

the area of fluid to move, thus $W_s \sim w\Delta e$. If the temperature is large enough, $k_BT > W_s$, then the thermal fluctuations are enough to depin the droplet. For lower temperatures, there will be a critical stripe width after which the droplet is pinned, and the depinning work will increase linearly with w. We must point out two restrictions to this simple model. First, in the absence of slippage only the contact line moves, in that case the energies involved when crossing from a hydrophilic to hydrophobic stripe or the opposite would be different. Second, as the stripe width becomes comparable to the droplet size we expect the depinning work to become independent of the stripe width, and converge toward the difference of adhesion energies between the two surfaces.

We now focus on the dynamics of the droplet after the depinning. For the two smallest stripe width, we do not observe any pinning, and $\langle v_{\mathrm{CM}} \rangle$ increases linearly with the bulk force. Assuming the model for the homogeneous substrates

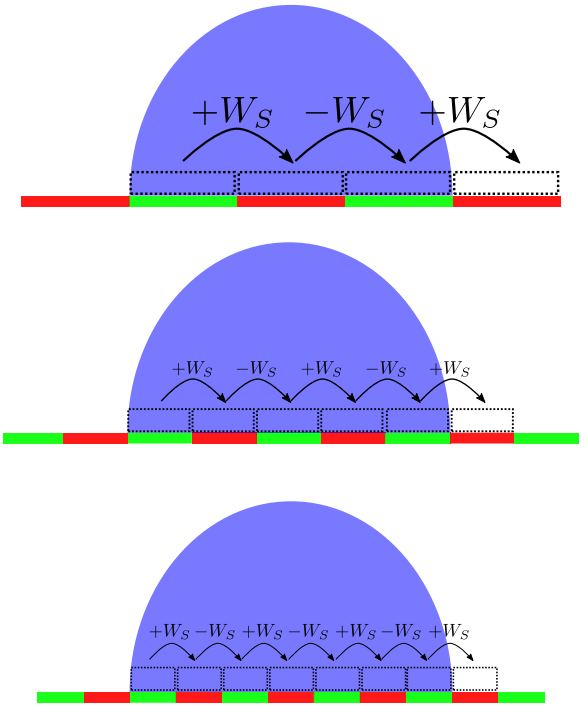

FIG. 10. An illustration for the depinning work W_s. A pinned droplet is in contact with n hydrophobic stripes and $n+1$ hydrophilic stripes, the extremities must therefore be hydrophilic stripes.

TABLE II. Molecular dynamics simulation results for polymer drops of $N = 50\,000$ atoms on chemically heterogeneous surfaces for different stripe widths.

$w(\sigma)$	$r_z\,(\sigma)$	$H\,(\sigma)$	$\delta\,(\sigma)$	$\gamma\,(m/\tau)$	$\gamma_{\mathrm{MD}}\,(m/\tau)$
1.26	27	59	74	60	56
2.52	27	58	64	68	96
3.78	27	59	62.5	68	81
5.04	26	57	62.5	71	83
7.56	26	57	62.5	71	71
10.08	27	58	62.5	71	57

is still valid, we perform linear fits on $\langle v_{\mathrm{CM}}\rangle$ and evaluate the effective damping coefficients. We give in Table II the results of the simulations and the value of γ obtained from the slip lengths calculations and geometry of the droplet with Eqs. (13) and (15). Again we notice that the dynamics is relatively well described in terms of the model. This corroborates the continuum results of Herde *et al.* [33] where the velocity of the droplet is extremely sensitive to the slip length. For small stripe widths, the fact that the substrate is chemically heterogeneous does not alter significantly the dynamics. Except for a smaller slip length δ, and thus a larger effective damping coefficient. Since the velocity profile derived for the homogenenous substrates still describes relatively well the dynamics on striped surfaces, we can assume that at least on average, the droplets motion can be described by a combination of sliding and rotation. This is due to the fact that while the surface is heterogeneous it is still smooth. Similarly, for the pinned droplets, after the critical force, for large enough force, we recover a linear regime for the velocity of the center of mass. We observe a sinusoidal variation of the velocity of the droplet as a function of time. Similar modulations of the center of mass velocity were observed in several other studies [28,30,31,33,35]. As the edge of the droplet crosses from a hydrophilic stripe to a hydrophobic one, the total surface energy increases since the interaction is less attractive, and consequently, the kinetic energy increases. We have evaluated the average velocity and surface potential energy as a function of the position of the center of mass with respect to the substrate. We averaged the results over the distance of two stripes for better statistics, the results are depicted in Figs. 11(a) and 11(b) for the two largest stripes at a force per atom of $F = 10^{-4}\ m\sigma/\tau^2$ and for $w = 3.78\ \sigma$ at $F = 1.5 \times 10^{-5}\ m\sigma/\tau^2$. When the surface energy is minimum, the center of mass of the droplet corresponds to the pinned position, in other words when it is in contact with one more hydrophilic stripe than a hydrophobic one. As the droplet crosses to a hydrophobic stripe its velocity decreases until it is in contact with one more hydrophobic stripe than a hydrophilic one, corresponding to the largest potential energy. Afterwards the velocity increases again. We notice that the modulation of the center of mass velocity does not affect significantly its mean value. Indeed, the linear fits in Fig. 7 and the corresponding results in Table II suggest that after the critical force the dynamics of the droplet can still be relatively accurately described by the model. This result is in contrast with the continuum of Sbragaglia *et al.* [35]. Indeed, their

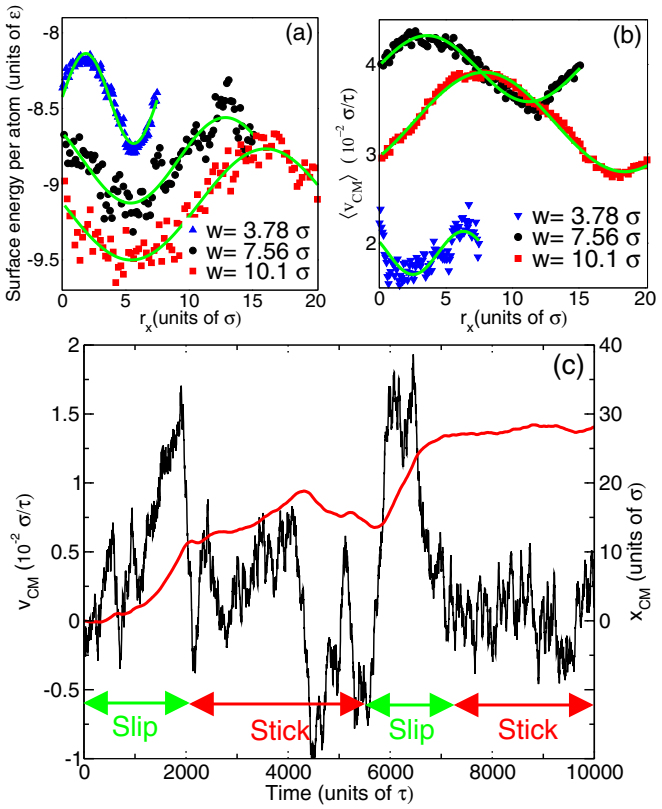

FIG. 11. (a) The surface energy per atom and (b) the averaged velocity of the center of mass as a function of the position of the center of mass. The energy was scaled by a factor 10^3. The plain lines correspond to sinusoidal fits. The center of mass velocity for $w = 3.78\sigma$ is multiplied by 5 for better visualization. (c) Velocity of the center of mass and position of the center of mass as a function of time for a typical trajectory in the stick-slip regime for a stripe width of $w = 10.1\ \sigma$.

results suggest an important increase in dissipation on striped surfaces, with the energy dissipation localized in time at the crossing of the boundaries. However, extreme deformations occurred during the dynamics, which does not occur for the small droplets considered here. Moreover, slippage was not taken into account, hence further hindering the crossing from one stripe to the other. For droplets at the nanoscale in the presence of slippage our results suggest that the dynamics after the depinning can still be relatively well described in terms of the model for homogeneous surface.

However, one would expect that for forces just above the critical force the dynamics would be consistent with stick-slip motion, in other words a succession of pinnings and depinnings. In that case, for a droplet in the pinned state, large thermal fluctuations allows to depin the droplet until it crosses to the next stripe and is pinned again. We have depicted such a trajectory in Fig. 11(c) for the largest stripe width. We observe that once the droplet is in the slip state it crosses rapidly one stripe and then becomes pinned. In the pinned state the position of the center of mass only fluctuates slightly, not enough to cross a stripe, after some time a large enough fluctuation permits the droplet to slip again and so on. We first remark that there is no need for vapor to observe

stick-slip dynamics as previously suggested [20]. However, we notice that the time between the successive depinnings varies wildly. Hence, once we consider time averages or the average on different trajectories one recovers a sinusoidal-like variation of the velocity as for the higher bulk forces. Since time-averaged molecular dynamics should correspond to continuum dynamics, this might explain why continuum studies observe an important slow down instead of a pinning of the contact line [28,33,62].

IV. CONCLUSION

In this paper we presented coarsed-grained molecular dynamics simulation of the statics and dynamics of cylindrical polymer droplets on chemically homogeneous and heterogeneous surfaces. The surfaces consist of two layers of *fcc* lattices which interact with a modified Lennard-Jones potential with the polymeric fluid. The hydrophobicity of the surfaces is tuned with an empirical parameter weighting the attractive term. Chemically heterogeneous surfaces can then be defined with stripes of different hydrophobicity. We first evaluated the equilibrium contact angle on different surfaces. We showed that at equilibrium the droplet deforms slightly to accommodate one extra hydrophilic stripe with respect to hydrophobic ones. As a result, at equilibrium, the droplet has to be in contact with an odd number of stripes. As the stripe width increases this results in relatively large differences of contact angle. However, on average we have observed that the Cassie-Baxter relation gives a good approximation of the equilibrium contact angle.

We then focused on the boundary condition, indeed at microscopic scales the fluid can slip on the solid surface. On smooth homogeneous surfaces this results in a combination of sliding and rotating motion for small droplets. We previously showed that on homogeneous surfaces, the steady-state velocity of the droplet scales linearly with the bulk force and depends only on its geometry, i.e., contact angle and size, and the amount of slippage at the surface [12]. For small stripe widths, this is still true as the fluid only sees an effective surface. Consequently, one can assume that the droplets still have a simple sliding and rotating motion. However, as the stripe width increases we noticed that the droplet becomes pinned until a sufficiently large force is exerted. We showed that the depinning force increases linearly with the stripe width. Since at equilibrium, the droplets extremities have to be on hydrophilic stripes, the net work required to depin the droplet is the work to move an amount of fluid from a hydrophilic stripe to an hydrophobic one, which in turn scales as the surface of the stripes as long as the stripe widths are smaller than the droplet. Once the droplet is depinned the steady-state velocity oscillates with time, consistent with the changes in surface energy when crossing different stripes. The velocity profile derived for homogeneous systems still predicts relatively well the center of mass velocity, suggesting that even though the velocity oscillates, it does not cause a noticeable dissipation source for the droplets we considered. Finally, between the pinned state and linear regime we observed a characteristic stick-slip regime where during the pinned state the position of the center of mass never crosses stripe while in the slip state, large thermal fluctuations can depin the droplets and permit to rapidly cross a stripe.

ACKNOWLEDGMENT

This research is financially supported by the Istanbul Technical University Scientific Research Fund (ITU-BAP) under Grant No. 38062.

[1] T. M. Squires and S. R. Quake, Rev. Mod. Phys. **77**, 977 (2005).
[2] R. Seemann, M. Brinkmann, T. Pfohl, and S. Herminghaus, Rep. Prog. Phys. **75**, 016601 (2012).
[3] J. ter Schiphorst, J. Saez, D. Diamond, F. Benito-Lopez, and A. P. H. J. Schenning, Lab Chip **18**, 699 (2018).
[4] V. Dugas, J. Broutin, and E. Souteyrand, Langmuir **21**, 9130 (2005).
[5] L. X. Kong, A. Perebikovsky, J. Moebius, L. Kulinsky, and M. Madou, J. Lab. Autom. **21**, 323 (2016).
[6] H. Zhou, R. Chang, E. Reichmanis, and Y. Song, Langmuir **33**, 130 (2017).
[7] H. M. Evans, E. Surenjav, C. Priest, S. Herminghaus, R. Seemann, and T. Pfohl, Lab Chip **9**, 1933 (2009).
[8] C. G. L. Furmidge, J. Colloid Sci. **17**, 309 (1962).
[9] P. Lenz and R. Lipowsky, Phys. Rev. Lett. **80**, 1920 (1998).
[10] H. Gau, S. Herminghaus, P. Lenz, and R. Lipowsky, Science **283**, 46 (1999).
[11] A. A. Darhuber and S. M. Troian, Annu. Rev. Fluid Mech. **37**, 425 (2005).
[12] J. Servantie and M. Müller, J. Chem. Phys. **128**, 014709 (2008).
[13] M.-C. Jullien, M.-J. Tsang Mui Ching, C. Cohen, L. Menetrier, and P. Tabeling, Phys. Fluids **21**, 072001 (2009).
[14] R. L.-Aguilar, R. Nistal, A. H.-Machado, and I. Pagonabarraga, Nat. Mater. **10**, 367 (2011).
[15] C. Duprat, S. Protiere, A. Y. Beebe, and H. A. Stone, Nature **482**, 510 (2012).
[16] H. Amini, E. Sollier, M. Masaeli, Y. Xie, B. Ganapathysubramanian, H. A. Stone, and D. Di Carlo, Nat. Commun. **4**, 1826 (2013).
[17] X. Yao, Y. Hu, A. Grinthal, T. S. Wong, L. Mahadevan, and J. Aizenberg, Nat. Mater. **12**, 529 (2013).
[18] E. Schaffer and P.-Z. Wong, Phys. Rev. Lett. **80**, 3069 (1998).
[19] J. Léopoldès and D. G. Bucknall, J. Phys. Chem. B **109**, 8973 (2005).
[20] H. Tavana, G. Yang, C. M. Yip, D. Appelhans, S. Zschoche, K. Grundke, M. L. Hair, and A. W. Neumann, Langmuir **22**, 628 (2006).
[21] S. Maheshwari, L. Zhang, Y. Zhu, and H.-C. Chang, Phys. Rev. Lett. **100**, 044503 (2008).
[22] D. Orejon, K. Sefiane, and M. E. R. Shanahan, Langmuir **27**, 12834 (2011).

[23] U. M. Mirsaidov, H. Zheng, D. Bhattacharya, Y. Casana, and P. Matsudaira, Proc. Natl. Acad. Sci. U.S.A. **109**, 7187 (2012).
[24] Y. H. Yeong, A. Milionis, E. Loth, and I. S. Bayer, Sci. Rep. **5**, 8384 (2015).
[25] M. E. R. Shanahan, Langmuir **11**, 1041 (1995).
[26] U. Thiele and E. Knobloch, New J. Phys. **8**, 313 (2006).
[27] U. Thiele and E. Knobloch, Phys. Rev. Lett. **97**, 204501 (2006).
[28] H. Kusumaatmaja, J. Léopoldès, A. Dupuis, and J. M. Yeomans, Europhys. Lett. **73**, 740 (2006).
[29] H. Kusumaatmaja and J. M. Yeomans, Langmuir **23**, 6019 (2007).
[30] X.-P. Wang, T. Qian, and P. Sheng, J. Fluid Mech. **605**, 59 (2008).
[31] T. Qian, C. Wu, S. L. Lei, X.-P. Wang, and P. Sheng, J. Phys.: Condens. Matter **21**, 464119 (2009).
[32] PH. Beltrame, P. Hänggi, and U. Thiele, Europhys. Lett. **86**, 24006 (2009).
[33] D. Herde, U. Thiele, S. Herminghaus, and M. Brinkmann, Europhys. Lett. **100**, 16002 (2012).
[34] S. Varagnolo, D. Ferraro, P. Fantinel, M. Pierno, G. Mistura, G. Amati, L. Biferale, and M. Sbragaglia, Phys. Rev. Lett. **111**, 066101 (2013).
[35] M. Sbragaglia, L. Biferale, G. Amati, S. Varagnolo, D. Ferraro, G. Mistura, and M. Pierno, Phys. Rev. E **89**, 012406 (2014).
[36] F. C. Wang and H. A. Wu, Sci. Rep. **5**, 17521 (2015).
[37] J. Zhang, F. Müller-Plathe, and F. Leroy, Langmuir **31**, 7544 (2015).
[38] M. Liu and X.-P. Chen, Phys. Fluids **29**, 082102 (2017).
[39] A. J. Briant, A. J. Wagner, and J. M. Yeomans, Phys. Rev. E **69**, 031602 (2004); A. J. Briant and J. M. Yeomans, *ibid.* **69**, 031603 (2004).
[40] G. S. Grest and K. Kremer, Phys. Rev. A **33**, 3628 (1986).
[41] K. Kremer and G. S. Grest, J. Chem. Phys. **92**, 5057 (1990).
[42] J. Baschnagel C. Bennemann, W. Paul, and K. Binder, J. Phys.: Condens. Matter **11**, 2179 (1999).
[43] J. Servantie and M. Müller, Phys. Rev. Lett. **101**, 026101 (2008).
[44] J. L. Barrat and L. Bocquet, Faraday Discuss. **112**, 119 (1999).
[45] L. Verlet, Phys. Rev. **159**, 98 (1967).
[46] C. Pastorino, T. Kreer, M. Müller, and K. Binder, Phys. Rev. E **76**, 026706 (2007).
[47] L. G. MacDowell, M. Müller, C. Vega, and K. Binder, J. Chem. Phys. **113**, 419 (2000).
[48] P. J. Hoogerbrugge and J. M. V. A. Koelman, Europhys. Lett. **19**, 155 (1992).
[49] P. Espanol and P. Warren, Europhys. Lett. **30**, 191 (1995).
[50] T. Soddemann, B. Dünweg, and K. Kremer, Phys. Rev. E **68**, 046702 (2003).
[51] S. Becker, H. M. Urbassek, M. Horsch, and H. Hasse, Langmuir **30**, 13606 (2014).
[52] T. Nishino, M. Meguro, K. Nakamae, M. Matsushita, and Y. Ueda, Langmuir **15**, 4321 (1999).
[53] A. B. D. Cassie and S. Baxter, Trans. Faraday Soc. **40**, 546 (1944).
[54] C. L. Navier, Mem. Acad. R. Sci. Inst. Fr. **6**, 389 (1823).
[55] L. Bocquet and J.-L. Barrat, Phys. Rev. Lett. **70**, 2726 (1993).
[56] L. Bocquet and J.-L. Barrat, Phys. Rev. E **49**, 3079 (1994).
[57] R. S. Voronov, D. V. Papavassiliou, and L. L. Lee, J. Chem. Phys. **124**, 204701 (2006).
[58] R. S. Voronov, D. V. Papavassiliou, and L. L. Lee, Chem. Phys. Lett. **441**, 273 (2007).
[59] N. V. Priezjev, A. A. Darhuber, and S. M. Troian, Phys. Rev. E **71**, 041608 (2005).
[60] Ho-Young Kim, Heon Ju Lee, and Byung Ha Kang, J. Colloid Interface Sci. **247**, 372 (2002).
[61] T. Podgorski, J.-M. Flesselles, and L. Limat, Phys. Rev. Lett. **87**, 036102 (2001).
[62] Q. Li, P. Zhou and H. J. Yan, Langmuir **32**, 9389 (2016).